Геология и геофизика, *т. 65, № 2, с. 288–302*, DOI: 10.15372/GIG2023170, EDN: BTLIOR
Поступила в редакцию 14.03.2023, принята в печать 01.09.2023 *Опубликована онлайн: 03.09.03*

УДК 534.647+553.982(549)

СЕЙСМОФАЦИАЛЬНЫЙ АНАЛИЗ, 3D КАРТИРОВАНИЕ ГОРИЗОНТОВ И ХАРАКТЕРИСТИКИ НЕФТЕМАТЕРИНСКИХ ПОРОД И ПОРОД КОЛЛЕКТОРОВ ПАЛЕОЦЕНОВОЙ ТОЛЩИ БАССЕЙНА ПОТВАР (*Пакистан*), С АКЦЕНТОМ НА ЕЕ ПОТЕНЦИАЛЬНУЮ НЕФТЕНОСНОСТЬ

Сайед Билавал Али Шах

University of Malaya, Kuala Lumpur, 50603, Malaysia

В данном исследовании представлен комплексный анализ нефтяного месторождения Балкассар в бассейне Потвар (*Пакистан*), на основе данных сейсморазведки, трехмерной модели приповерхностного горизонта, а также геохимических и петрофизических данных. Оценка геохимических свойств свиты Локхарт с использованием бурового шлама выявила устойчивое относительно низкое или умеренное содержание общего органического углерода (ООУ). Значения S2 ее отложений предполагают их хороший генерационный потенциал и смешанный состав керогена (типы II и III). С помощью сейсмофациального анализа выделено пять различных категорий отложений с параллельными параметрами. Горизонты от нижней перми до эоцена имеют различную амплитуду, преимущественно параллельно-волнистую внутреннюю конфигурацию, а также в основном пластовую или клиновидную геометрию, что дает представление о стратиграфии толщи. Интерпретация 3D сейсмических данных выявила структурные особенности свиты Локхарт с выраженным северо-западным падением и более пологим юго-восточным наклоном. Крылья свиты секутся обрамляющими ее разломами. На северо-западе свита граничит с разломом, что создает благоприятные предпосылки для накопления углеводородов. По данным петрофизического анализа средняя пористость отложений составляет 9.17 %. Свита сложена преимущественно известняками; средняя водонасыщенность ее отложений составляет около 25.29 %, а насыщенность углеводородами — примерно 74.71 %, что способствует ее коллекторским свойствам. Свита Локхарт в бассейне Потвар является потенциально нефтегазоносной, хотя генерационный потенциал ее нефтематеринских пород ограничен. Проведенное исследование дает более глубокое представление о сложной геологической структуре месторождения Балкассар и вносит вклад в разработку методов нефтепоисковых работ в бассейне Потвар.

Свита Локхарт, нефтематеринская порода, бассейн Потвар

SEISMIC FACIES ANALYSIS, 3D HORIZON MAPPING, SOURCE AND RESERVOIR ROCK CHARACTERISTICS OF THE PALEOCENE SEQUENCE IN POTWAR BASIN, PAKISTAN: WITH EMPHASIS ON PETROLEUM POTENTIAL PROSPECT

Syed Bilawal Ali Shah

This study presents a comprehensive analysis of the Balkassar oilfield in the Potwar Basin, Pakistan. It integrates seismic reflection data, a 3D subsurface horizon model, and geochemical and petrophysical data. Evaluating the Lockhart Formation's geochemical properties using well cuttings reveals consistent patterns of relatively low to fair total organic carbon (TOC). S2 values suggest a fair generation potential with a mixed Type II–III kerogen composition. Seismic facies analysis identifies five distinct categories with parallel attributes. Horizons from lower Permian to Eocene show varying amplitudes and prevalent parallel to wavy internal configurations. Geometries, mainly sheet-to-wedge, enhance stratigraphic understanding. The 3D seismic interpretation reveals the Lockhart Formation's structural traits, with pronounced northwest dip and gentler southeast inclination. Faults flanking the formation truncate its limbs. A significant contour closure in the northwest, confined by fault boundaries, signifies attractive hydrocarbon potential. Petrophysical analysis indicates an average 9.17% porosity. Dominated by limestone, the formation shows average water saturation of around 25.29% and hydrocarbon saturation of roughly 74.71%, indicating favorable reservoir properties. The Lockhart Formation holds promise as a reservoir rock within the Potwar Basin, though its source rock suitability is limited. This study enhances understanding of Balkassar's geological complexities and contributes to knowledge of hydrocarbon exploration in the Potwar Basin.

Lockhart Formation, Potwar Basin, Source rock

INTRODUCTION

The Potwar Basin, located in Pakistan, stands as a significant hub for oil and gas production. Numerous researchers, including Imtiaz et al. (2017), Fazeelat et al. (2010), Ihsan et al. (2022), and Shah (2022), have made substantial contributions to our understanding of the hydrocarbon reserves within this basin. While the primary nature of hydrocarbon traps in the Potwar Basin is structural, the presence of stratigraphic traps has also been noted (Yasin et al., 2021; Ma et al., 2023; Yuan et al., 2023).

✉e-mail: bilawalshah22@yahoo.com

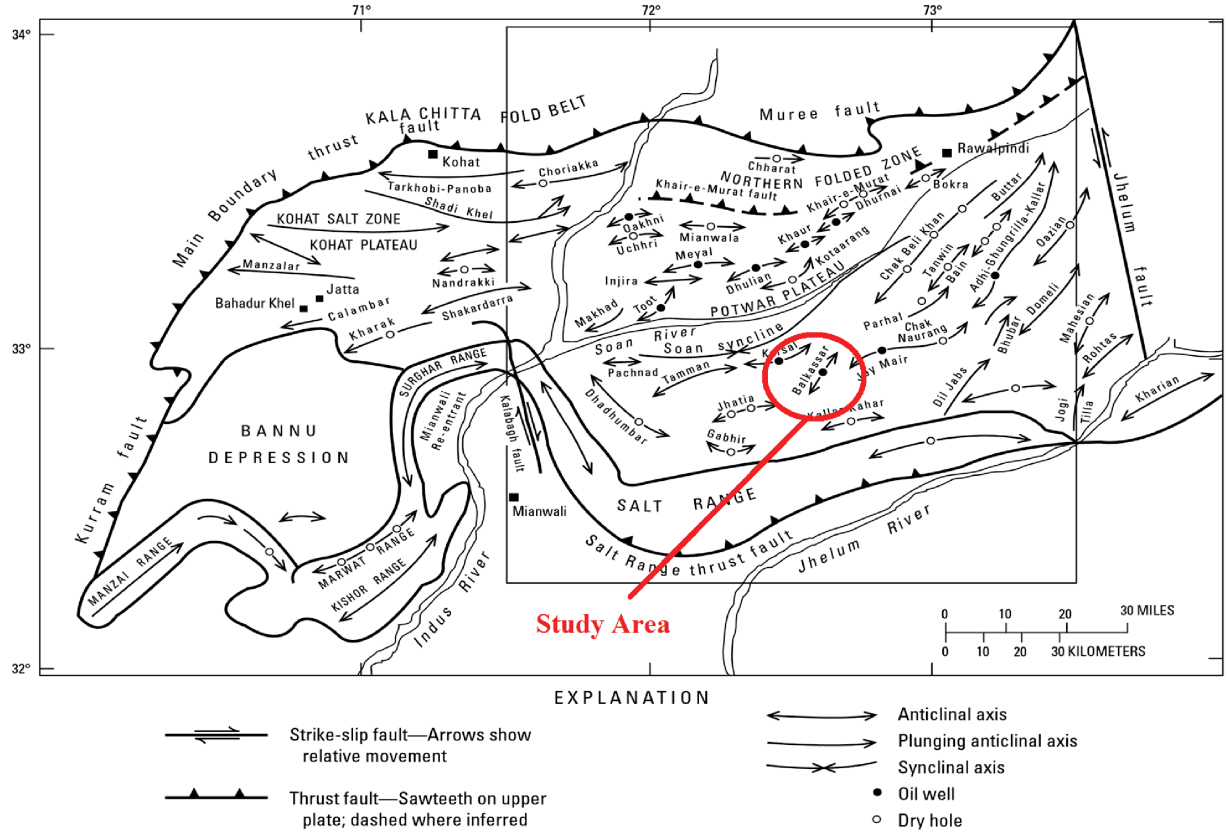

Fig. 1. Structural map showing different tectonic divisions, major structures and study area in Potwar subbasin. (He et al., 2021; Huang et al., 2021; Li et al., 2021, 2022a).

Fazeelat et al. (2010) conducted a comprehensive study of the shallow marine sediments within the Potwar Basin, unearthing a wealth of organic material. This discovery underscores the importance of creating and analyzing 3D models that map the Lockhart Formation horizon, both temporally and spatially. Additionally, it emphasizes the necessity of comprehending the qualities of source and reservoir rocks within the Balkassar oilfield of the Potwar Basin.

This research introduces a novel dimension by employing seismic facies analysis to identify seismic facies. The investigation integrates seismic data for the formulation of 3D horizon distribution models, coupled with a meticulous examination of well-cutting samples and well logs. These analyses facilitate the interpretation and distribution of subsurface horizons, evaluation of source rock potential, assessment of thermal maturity, determination of kerogen types, and characterization of petrophysical properties. The novelty of this study lies in its fusion of three distinct approaches to scrutinize and assess the horizon, as well as the attributes of source and reservoir rocks. Such a holistic approach is pivotal in comprehending the petroleum system. Prior researchers have concentrated on different formations, employing diverse methodologies. For instance, Shah and Shah (2021) developed comprehensive models of the entire structure, with a specific focus on salt diapirs. Fazeelat et al. (2010) probed into the source rock properties of the Sakesar Formation, while Iqbal et al. (2015) explored crustal shortening and identified four significant faults. Masood et al. (2017) delved into the Tobra and Khewra formations.

Table 1. **Reservoirs' porosity as described qualitatively by Rider (1986)**

Average porosity with qualitative description
Porosity ranging from 0 to 5% is considered Negligible
Porosity ranging from 5 to 10% is considered Poor
Porosity ranging from 10 to 20% is considered Good
Porosity ranging from 20 to 30% is considered Very good
Porosity greater >30% is considered Excellent

Nevertheless, a noticeable dearth of information pertains to the interpretation of the Lockhart Formation's subsurface distribution within the Balkassar oilfield, along with the requisite knowledge regarding source and reservoir rock attributes that are indispensable for comprehending the formation's potential and characteristics. Consequently, this study assumes paramount importance in filling these lacunae. It should be underscored that the Balkassar oilfield resides within the broader confines of the Potwar Basin (Fig. 1).

The aim of this study is to reveal the 3D models of the Lockhart Formation, analyze the ability of source and reservoir rocks to generate hydrocarbons, determine the type of kerogen present, assess the thermal maturity of rocks as potential sources of hydrocarbons, and identify possible hydrocarbon prospects. The outcomes of this research will directly assist upcoming oil and gas companies in their hydrocarbon exploration efforts. The study will significantly enhance the field by offering valuable insights and aiding in the comprehension of the Lockhart Formation's diverse characteristics, which could contribute to future hydrocarbon exploration and production.

In this study, we've merged our ongoing work with prior investigations carried out by Shah (2022), Shah and Abdullah (2016, 2017), and other researchers including Masood et al. (2017) and Ahsan et al. (2012). This collaborative approach enables us to meticulously analyze the Lockhart Formation's geometry and its potential as a source or reservoir rock within the Balkassar oilfield. As the study by Ahsan et al. (2012) have also recommended to investigate Balkassar anticline at the Paleocene level (Lockhart Formation).

We evaluated reservoir rock attributes using a set of original wireline logs from Balkassar well OXY-01, presented in a LAS file format. These raw logs were processed to provide pertinent information for estimating the presence of subsurface oil and gas. Descriptive assessments of reservoir features were based on criteria outlined by Rider (1986) and Shah and Shah (2022) (Table 1).

GEOLOGICAL SETTING

The Potwar Basin possesses several significant features, encompassing inner and outer folded zones, a platform, and a foredeep marked by depressions (Zhao et al., 2020; Shah, 2023; Zhang et al., 2022b; Zhao et al., 2022). The specific study area being examined is referred to as the Balkassar oilfield.

Table 2. **Potwar Basin general stratigraphy (Xu et al., 2021; Shah, 2022; Wu et al., 2022b; Liu et al., 2023d)**

AGE/EPOCH		LITHOLOGY	FORMATION	LITHOLOGY DESCRIPTION
Neogene	Pliocene	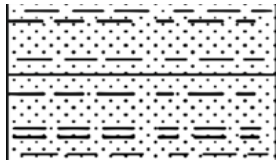	Nagri Chinji	Sandstone, sandstone and clay
	Miocene Oligocene		Kamlial Murree	Sandstone, sandstone, limestone
Oligocene	**Unconformity**			
Paleogene	Eocene	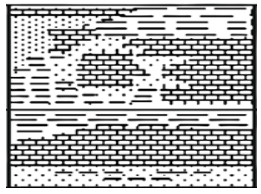	Chorgali* Sakesar*#	Limestone, limestone
	Palaeocene		Patala # Lockhart #* Hangu #*	Shale, limestone, sandstone
Mesozoic and Late Permian	**Unconformity**			
Jurassic		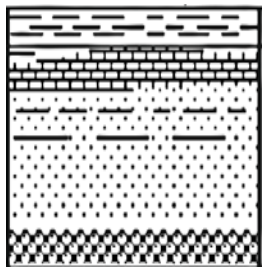	Datta	Sandstone, shale
Permian	Early Permian		Chhidru Wargal Amb Sardhai Warcha Dandot Tobra	Sandstone, limestone, limestone, siltstone, interbeds of sandstone, shale interbeds of sandstone, sandstone and conglomerate.
Carboniferous to Ordovician	**Unconformity**			
Cambrian to Precambrian	Cambrian	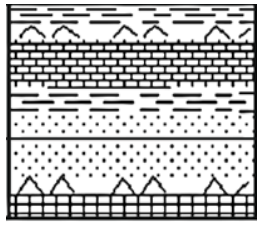	Baghanwala Jutana Kussak Khewra	Shale, dolomite, sandstone and siltstone, shale interbeds of dolomite and siltstone
	Infra-Cambrian		Salt Range	Marl, claystone and siltstone, salt
Legends	* Reservoir rocks		# Source rocks	

The Potwar Basin is geographically divided into two segments by the Indus and Jhelum rivers, as well as the Salt Range and the Kalachitta-Margalla hill ranges (Shah and Abdullah, 2017; Chen et al., 2023; Cheng et al., 2023; Dang et al., 2023). This basin is characterized by intricate and compact east-west folds that incline southward and are influenced by steep-angle faults. In the northern section of the basin, notable deformation is evident (Kazmi and Jan, 1997; Kazmi and Abbassi, 2008; Shah, 2009; Aadil and Sohail, 2014; Riaz, 2022; Shah, 2023). However, in the eastern portion, the orientation of the folds abruptly shifts towards the northeast, and the structures consist of tightly compressed large synclines and anticlines. Moving to the western part, numerous gentle and broad east-west folds are observed (Zahid et al., 2014; Li et al., 2022b; Peng et al., 2022; Shah, 2023; Wang et al., 2023).

OVERVIEW OF THE POTWAR BASIN'S SOURCE AND RESERVOIR ROCKS

The Potwar Basin is recognized for hosting several established source rocks, including the Sakesar, Hangu, Patala, and Lockhart formations (Ren et al., 2022; Xu et al., 2022a; Liu et al., 2023a) (Table 2). In terms of reservoir rocks, the basin encompasses various formations, which consist of Cambrian sandstones from alluvial and shoreface environments, Miocene alluvial sandstones, continental sandstones from the Jurassic and Permian periods, and shelf carbonates from the Paleogene period (Aadil and Sohail, 2014; Kazmi and Abbassi, 2002; Zhou et al., 2022; Li et al., 2022c; Xiao et al., 2023). Furthermore, the Potwar Basin has yielded oil and gas from reservoir rocks such as Tobra, Wargal, Amb, Cambrian Khewra, Jutana, Kussak, Jurassic Dutta, Khairabad, Lockhart, Nammal, Sakesar, Margalla Limestone, Chorgali, Bhadrar, and Murree (Zahid et al., 2014; Zhou et al., 2021d; Sun et al., 2023a, b).

Regarding oil and gas exploration, the discovered oilfields within the Potwar Basin are typically associated with structural features like popup structures, faulted anticlines, or fault-block traps (Xu et al., 2022b; Wu et al., 2022a; Liu et al., 2023c).

MATERIAL AND METHODS

The methodologies employed in this study encompass the utilization of computer-based Petrel software for generating 3D models and performing interactive petrophysical analysis, along with laboratory testing of

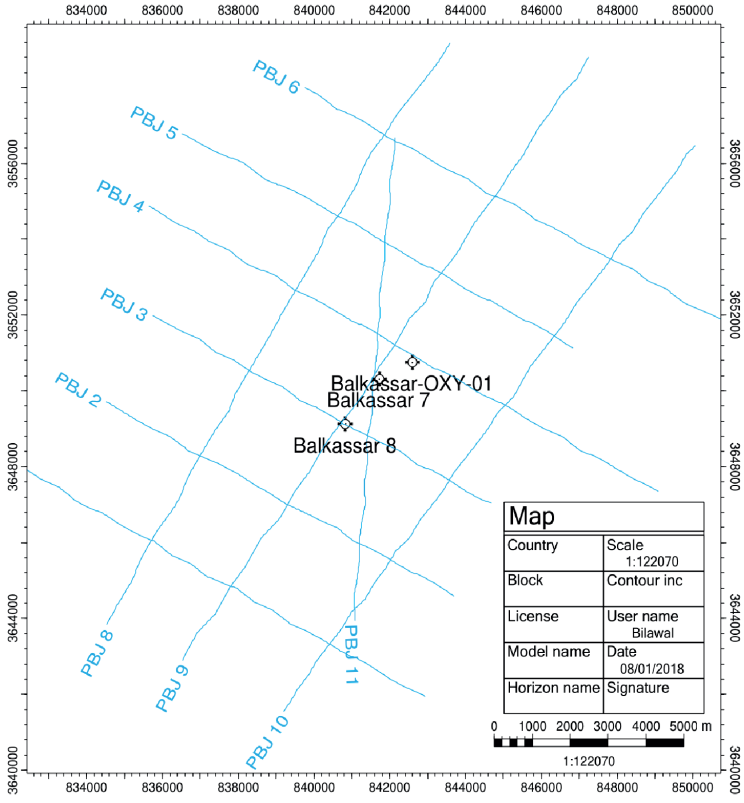

Fig. 2. Base-map showing wells location and seismic grid lines.

samples. The data used for constructing and interpreting the 3D models include: (i) a base map, (ii) seismic data consisting of eleven seismic dip and strike lines, and (iii) well log data extracted from Balkassar-OXY-01 (depicted in Fig. 2). Schlumberger Petrel software played a role in seismic structural interpretation, horizon mapping, and identifying potential prospects.

The seismic sections' velocities were scrutinized through average, mean, and interval velocity analyses. The complexity of the velocity studies and the depth surface presentation through Petrel software (Schlumberger) led to the inclusion of depth surface maps without the comprehensive analyses. Domain conversion facilitated the assessment of diverse data domains, primarily converting depth and seismic data from the time domain to the depth domain. The process of transitioning data between domains involved two steps: 1) developing the velocity model to depict subsurface velocity fluctuations, and 2) depth conversion, which involved moving data across domains using the velocity model.

A collection of twenty well cutting samples was procured from the Balkassar OXY-01 well in Balkassar, with sediment samples gathered at intervals of 1.2–2 m. Further information about these samples is available in Table 4. In this study, a petrophysical approach was employed to evaluate the reservoir potential of the Lockhart Formation, using a set of well logs from the Balkassar OXY-01 well. The assessment of reservoir rock properties involved the technique formulated by Hartmann and Beaumont (1999), as well as the methodology introduced by Shah (2022). The analysis of wireline logs encompassed gamma-ray logs, density logs, neutron logs, spontaneous potential logs, and resistivity logs. Parameters such as formation water resistivity, porosity, water saturation, and hydrocarbon saturation were also computed. These characteristics play a pivotal role in the evaluation of the hydrocarbon potential within reservoir rocks.

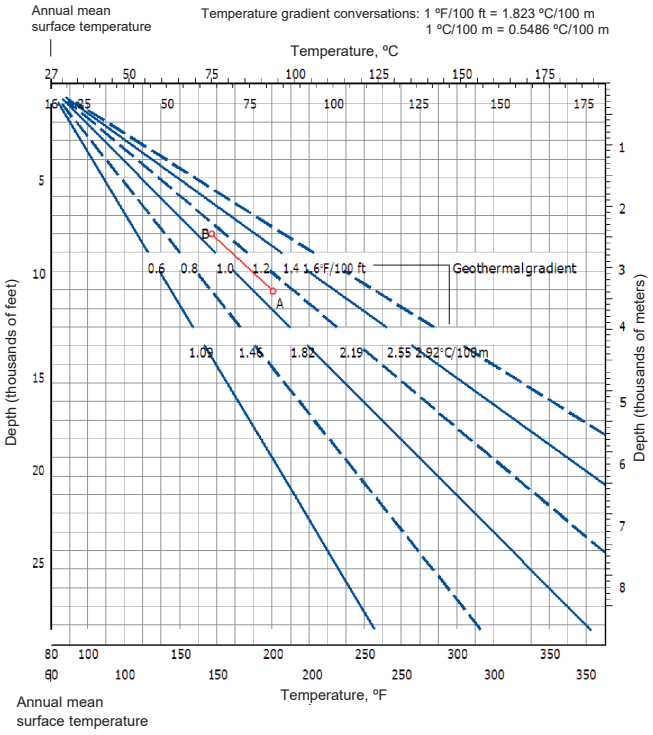

Fig. 3. Temperature of the formation at various depths (Zhou et al., 2022).

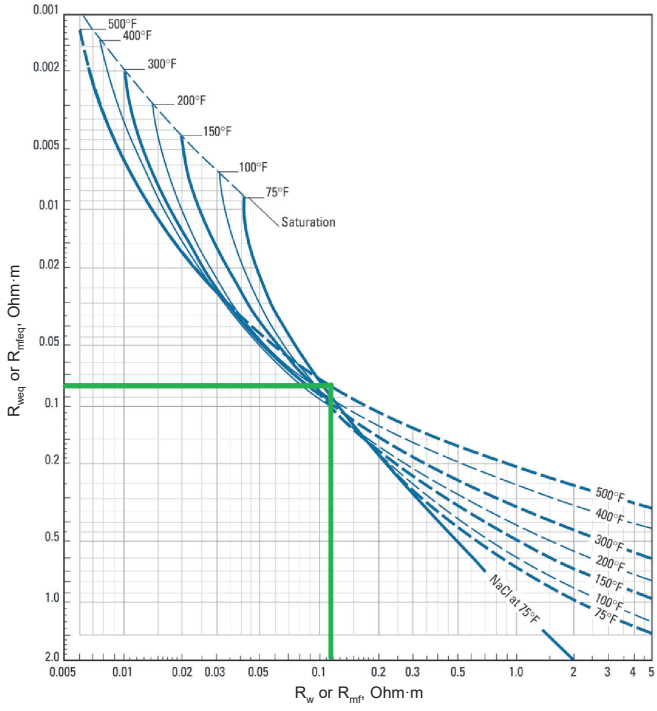

Fig. 4. R_w determined by determining R_{we} (Liu et al., 2021; Yang et al., 2022; Yin et al., 2023a).

SEISMIC REFLECTION FACIES ANALYSIS

The seismic facies study involves the interpretation and description of seismic features, including continuity, amplitude, and configuration. In this investigation, the PBJ-04 seismic dip line was utilized to identify various seismic facies in the Balkassar subsurface. This seismic line was chosen as a reference line because it runs along the top of the Balkassar anticline and is close to the Balkassar-OXY-01 well, which is the deepest well in the Balkassar oilfield.

The approach employed for seismic facies analysis in this study was adapted from Futalan et al. (2012), who used four reflection properties to differentiate between seismic facies on seismic reflections. These properties include:

1. Internal configuration;
2. Reflector continuity;
3. Amplitude;
4. External geometry.

The term "internal configuration" refers to the internal bedding patterns, such as convergent, wavy, oblique, parallel to wavy, and parallel to subparallel. "Reflector continuity" and "lateral continuity of strata" represent the continuity of reflectors and lateral extent of the strata, respectively. "Amplitude" refers to properties such as bedding thickness, spacing, density contrast, and velocity.

GEOMECIAL ANALYSIS

The well cutting samples were initially crushed into fine particles, each measuring less than 200 mesh. Following that, the measurement of TOC was carried out using LECO elemental analyzers, specifically the CS-125 model. Pyrolysis analysis was conducted using the Rock-Eval VI equipment. About 100 mg of the crushed samples underwent pyrolysis analysis within a helium atmosphere, and they were heated to a temperature of 600 °C. This pyrolysis process yielded three significant parameters: S1 (total free petroleum), representing the amount of hydrocarbons; S2, which indicates the quantity of hydrocarbons generated through thermal cracking; and T_{max}, as detailed by Shah and Shah (2021). In addition to these, other crucially important parameters that were calculated encompassed the hydrogen index and production yield.

WELL LOG ANALYSIS

The section below describes how to obtain various parameters from the well logs.

The following log track parameters were directly read, formation depth in ft. Bulk resistivity, neutron porosity, bulk density of formation and spontaneous potential values at various points.

Hydrocarbon Saturation (SH)

Schlumberger log interpretation charts were utilized in conjunction with multiple equations to determine certain required data from well in the Lockhart Formation to estimate the reservoir potential. The graphs and equations were used together in the following process:

Formation temp was calculated using Figs. 3, 4 and following equation:

$$Tf = Ts + Df\ (BHT\text{-}Ts/TD)$$

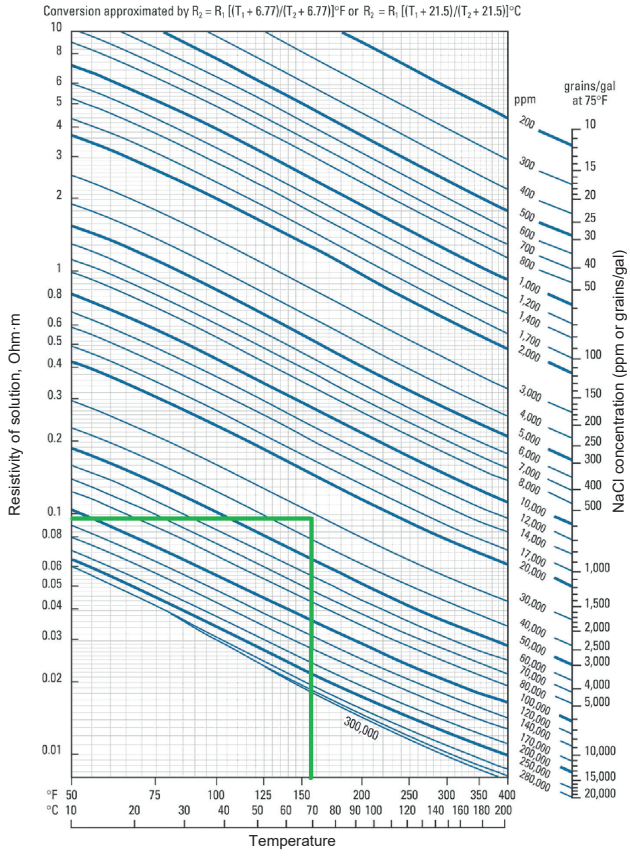

Fig. 5. R_w determined by determining R_{we} (Schlumberger, 1977).

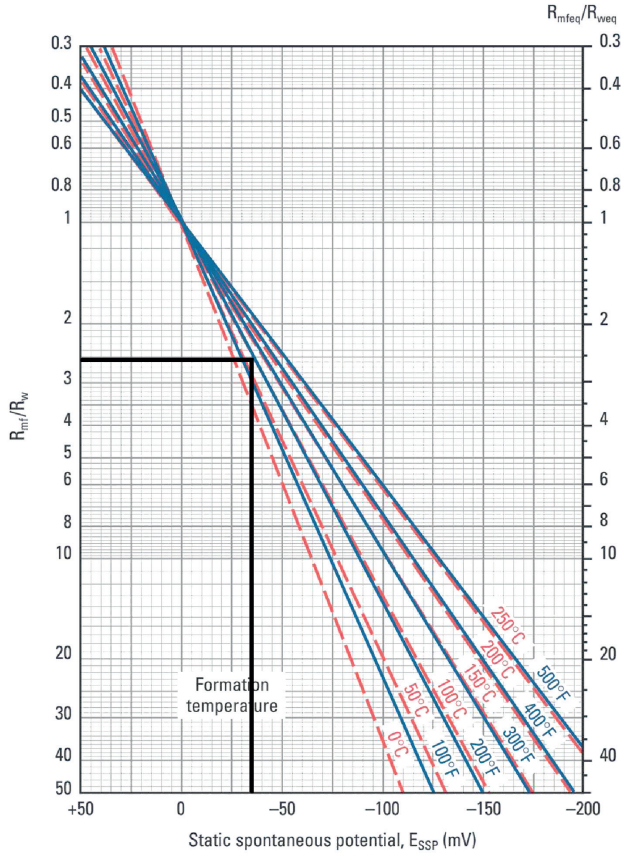

Fig. 6. R_{mf} and R_{we} correction according to temperature (Yu et al., 2021; Liu et al., 2022; Yang et al., 2023).

R_{mf} and R_m were corrected (Fig. 5).
S_p values were read from logs directly.
R_{mf}/R_{we} ratio was calculated (Fig. 6).
The R_{we} was calculated by R_{mf}/R_{we} ratio.
$R_{we} = R_{mfeq}/(R_{mfeq}/R_{we})$
Water saturation was calculated using Archie's equation:

$$S_w = \sqrt{\frac{R_w}{\phi^m \cdot R_t}}.$$

Hydrocarbon saturation was calculated using equation SH = 1–S_w.

RESULTS AND DISCUSSION

3D subsurface horizon maps. The Lockhart Formation exhibits faulting in the northwest corner, while it is distributed uniformly across the remaining area. The contour lines present minimal depth variation, except in the northwest corner. This discrepancy is attributed to the Lockhart Formation's potential uplift from its original depth, primarily due to the pressures exerted by the Himalayan orogenic belt, movement of the Indian plate, and the uplift of the Salt Range (as depicted in Fig. 7*a*). The contour map of the Lockhart Formation illustrates a relatively level portion of the Earth's crust (depicted in Fig. 7*a*). Broader contours in the northwest signify gentler inclines of the formation, whereas the closer contours in the southeast indicate the presence of thrust faults. Both the time and depth contour maps exhibit a level crystal segment (illustrated in Fig. 7*a*, *b*). Analysis of the contour lines reveals that the limbs in the northwest exhibit a steep dip of 65° to 75°, in contrast to the more gradual incline of the limbs in the southeast.

Total organic carbon and Rock-Eval Pyrolysis. Typically, TOC is used as an indicator of rock richness. According to Hunt (1996), clastic rocks should have a TOC value of 1.0% or higher to qualify as a source rock. Sediments from the Lockhart Formation exhibit a range of TOC content from 0.82 to 1.19% (wt.%). All of the samples show poor to fair TOC content.

S2, which is produced during pyrolysis, is the most useful parameter for estimating hydrocarbon generative potential (Peters and Cassa, 1994; Zhang et al., 2022a; Zhan et al., 2022; Zhou et al., 2022). Bordenave et al. (1993) and Shah and Abdullah (2017) state that a good petroleum generation capacity requires at least 5 mg HC/g S2. The S2 values of Lockhart Formation sediments ranged from 3.21 mg/g to 4.33 mg/g. The S2 vs TOC cross plot (Fig. 8) indicates a fair petroleum generation potential.

The migration index (S1/TOC) can be used to differentiate between indigenous and migrated petroleum (Zhou et al., 2021a, 2022; Zheng et al., 2023). The migration index S1 vs TOC plot (Fig. 10) indicates the presence of indigenous hydrocarbons.

Kerogen Type. The Hydrogen Index (HI) was utilized to assess the kerogen types in the formations, as it is considered the most important index for this purpose (Peters, 1986; Ren et al., 2023; Yao et al., 2023; Yin et al., 2023b). The HI values for the Lockhart Formation ranged from 300 to 410 mgHC/g TOC. HI vs T_{max} plots were constructed for kerogen classification. The majority of sediments investigated in all formations

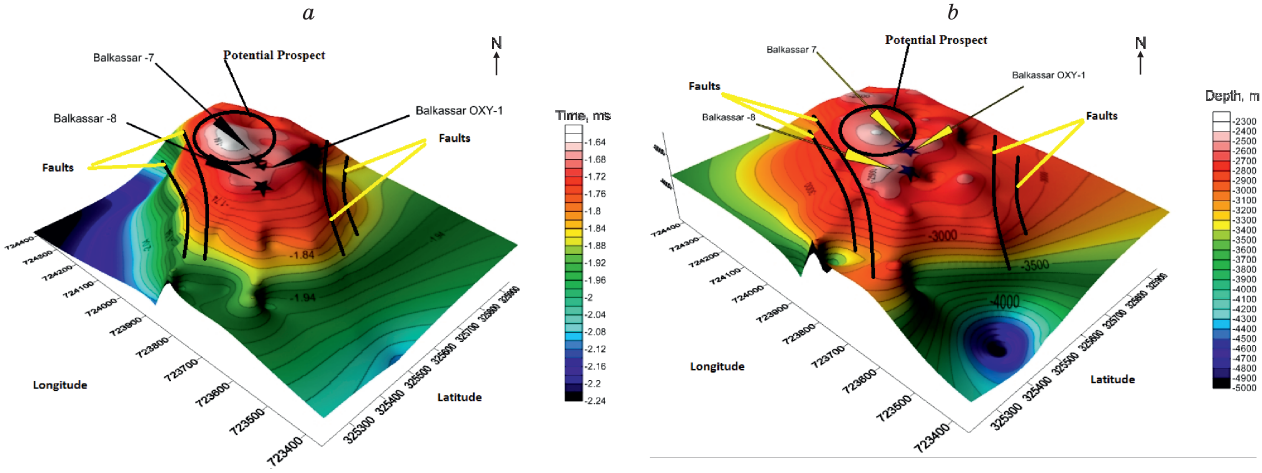

Fig. 7. 3D time contour map of Lockhart Formation (*a*), 3D depth contour map of Lockhart Formation (*b*).

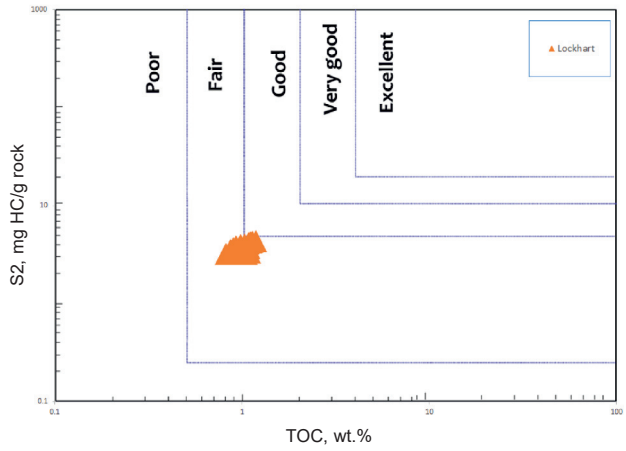

Fig. 8. Graph showing S2 versus total organic carbon for the analyzed samples.

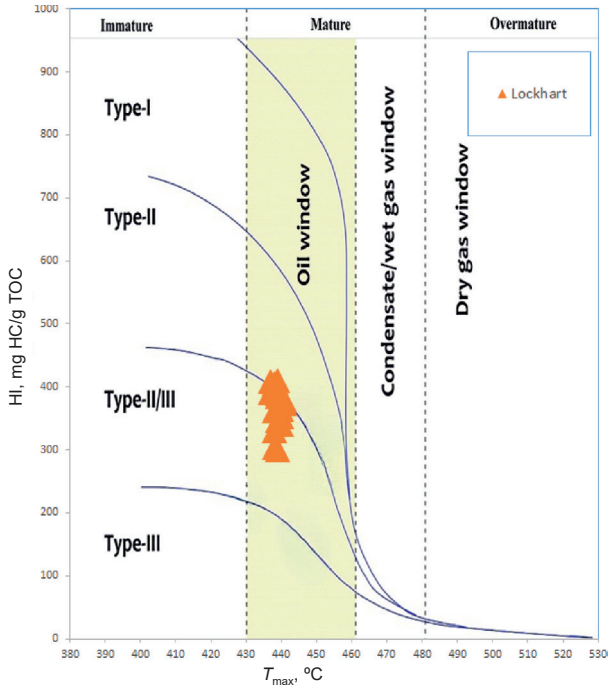

Fig. 9. HI versus T_{max} plot (Liu et al., 2023b; Zhou et al., 2021b, c).

showed mixed Type-II/III kerogen. The identification of kerogen type based on S2 vs TOC plots was consistent with the interpretation of the Van Krevelen diagrams (Fig. 11).

Thermal Maturity. For thermal maturity including T_{max} values, vitrinite reflectance (R_o, %), and Production Index were used for thermal maturity. Oil with vitrinite reflectance values varying from 0.6–1.3% Ro is thermogenic oil (Bordenave, 1999; Yin et al., 2023c).

Vitrinite reflectance values of the Lockhart Formation sediments ranged between 0.71–0.78% R_o (Table 4) and T_{max} varies between of 437–441 °C (Tables 3 and 4) showing peak of oil generation window (Fig. 11).

In terms of organic matter maturity, if the Production Index (PI) levels are below 0.05, samples may be considered immature and may have produced little to no hydrocarbons. Furthermore, samples with PI values between 0.05 and 0.10 can be regarded as having very limited oil production, potentially indicating entry into the wet gas zone. Finally, if PI readings exceed 1.0, the kerogen's capacity to produce hydrocarbons may have been depleted.

In this study, PI values for Lockhart Formation samples mostly varied between 0.20–0.33, thus also indicating maturity level (oil window) (Fig. 12).

Seismic facies identified. The approach outlined by Futalan et al. (2012) was employed to determine seismic facies. Following the meticulous identification of horizons, incorporating well tops and generating synthetic seismograms, the seismic facies within these horizons were delineated. Within the study area, five distinct seismic facies (designated as A, B, C, D, and

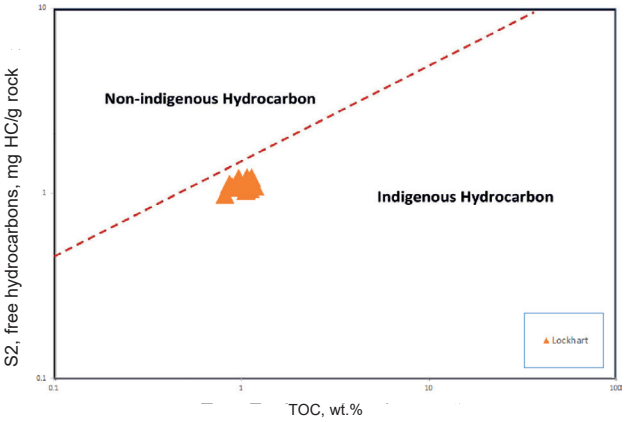

Fig. 10. S1 versus TOC plot.

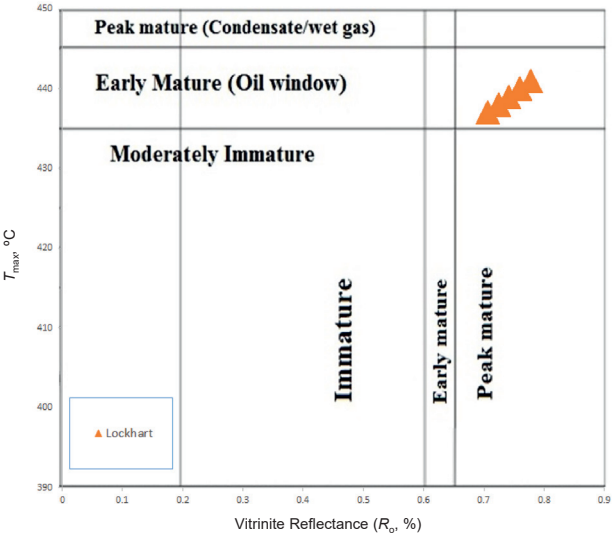

Fig. 11. Plot of T_{max} versus Vitrinite Reflectance (R_o) showing the maturity levels.

Table 3. **Summary of analyzed sediments in Balkassar-OXY-01 well**

Formation and number of samples	Depth, m	Petroleum potential				Maturity of sample	Quality of OM	Kerogen type	Source rock generative potential
		TOC, wt.%	S1	S2	S3	T_{max}, °C	HI		
Lockhart (20)	2624–2647	0.82–1.19	0.98–1.21	3.21–4.33	0.47–0.83	437–441	30–410	Mixed type II/III	Fair

Table 4. **Analyzed sediments data of Lockhart Formation from Balkassar-OXY-01 well**

Formation	TOC, %	T_{max}, °C	S1	S2	S3	PI	HI	OI	S2/S3	VR
Lockhart	1.1	439	1.12	3.3	0.52	0.31	300	47.3	6.34	0.74
	1.06	438	1.03	3.21	0.48	0.24	303	45.3	6.68	0.72
	0.9	437	1.08	3.67	0.47	0.33	408	52.2	7.80	0.71
	0.97	438	1.2	3.21	0.65	0.27	331	67	4.93	0.72
	1.12	440	1.06	4.2	0.74	0.2	375	66.1	5.67	0.76
	0.98	438	1.12	3.97	0.65	0.22	405	66.3	6.10	0.72
	1.08	439	1.21	4.16	0.54	0.23	385	50	7.70	0.74
	1.11	441	1.11	4.2	0.81	0.31	378	73	5.18	0.78
	1.19	440	1.09	4.33	0.73	0.2	364	61.3	5.93	0.76
	1.07	439	1.05	3.7	0.65	0.22	346	60.7	5.69	0.74
	0.96	440	1.07	3.64	0.62	0.23	379	64.6	5.87	0.76
	0.87	438	1.12	3.51	0.78	0.24	403	89.7	4.5	0.72
	1.03	439	1.08	4.01	0.81	0.21	389	78.6	4.95	0.74
	0.82	437	0.98	3.21	0.73	0.23	391	89	4.39	0.71
	0.93	440	1.08	3.28	0.82	0.25	353	88.2	4.1	0.76
	1.14	441	1.21	4.25	0.77	0.22	373	67.5	5.51	0.78
	1.09	440	1.18	3.7	0.74	0.28	339	67.9	5.01	0.76
	0.93	439	1.09	3.81	0.83	0.22	410	89.2	4.59	0.74
	1.1	440	1.12	4.21	0.76	0.21	383	69.1	5.53	0.76
	1.07	438	1.13	3.87	0.75	0.23	362	70.1	5.16	0.72

E) were identified (as listed in Table 5 and illustrated in Fig. 13). These facies generally display parallel distribution patterns and exhibit amplitudes ranging from moderate to high within the lower Permian to Eocene layers. While the Cambrian and lower Permian successions exhibited salt diapir growth originating above the basement horizon, a noteworthy continuity is observed within the Paleocene, Eocene, and Miocene successions. Across the majority of horizon sequences, internal configurations are primarily either parallel or wavy, with the exception of the Lower Miocene Chorgali horizon at the base (as shown in Fig. 14). Moreover, all successions consistently display an external geometry described as sheet-like to wedge-shaped.

Reservoir potential. For a quantitative interpretation of the reservoir, reservoir parameters derived from petrophysical analysis methods were used. Table 6 presents the estimated petrophysical characteristics of the Lockhart Formation. The calculated average porosity was 9.17%, indicating a poor to moderate reservoir potential. The average water saturation was 25.29%, while the average hydrocarbon saturation was 74.71%. Based on the criteria provided by Rider (1986) and Shah and Shah (2021), these values suggest that the reservoir has an average to good hydrocarbon potential (Table 1).

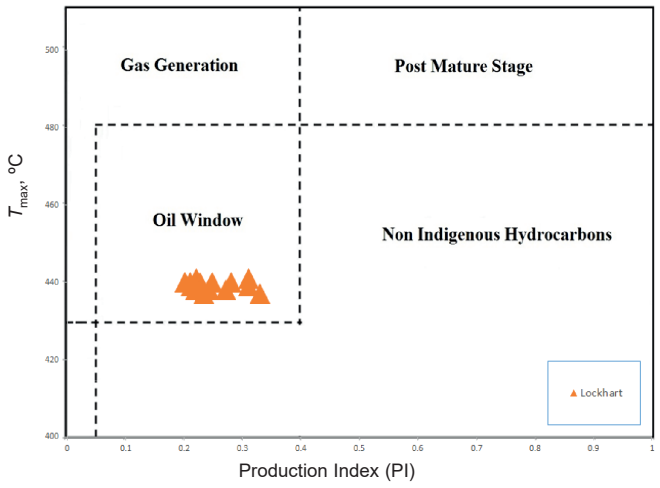

Fig. 12. T_{max} vs PI plot.

Table 5. **Seismic facies identified**

Seismic facies		Reflection attributes a) external geometry; b) internal configuration; c) continuity; d) amplitude strength.	Age
A	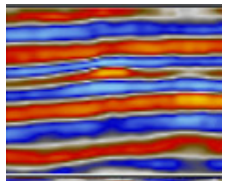	a) sheet to wedge; b) parallel to wavy; c) high continuity; d) moderate to high.	Paleocene–Eocene
B	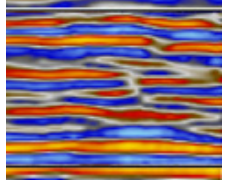	a) sheet to wedge; b) parallel to wavy; c) semi-continuous to high continuity; d) moderate to high.	Miocene
C	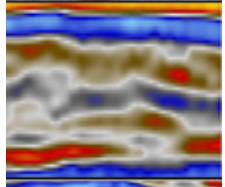	a) sheet to mound; b) wavy to hummocky; c) disrupted to discontinuous; d) moderate to high.	Lower Miocene
D	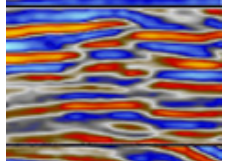	a) sheet to wedge; b) parallel to subparallel; c) semi-continuous to disrupted; d) low to moderate.	Precambrian–lower Permian
E	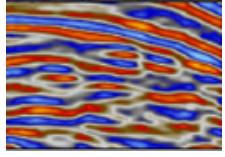	a) lens to wedge; b) subparallel to convergent to oblique; c) semi-continuous to high continuity; d) low to moderate.	Lower Permian

CONCLUSIONS

Following is a summary of the key findings from the interpretation and evaluation of the Lockhart Formation utilizing 3D horizon distribution models, prospective prospects, geochemical and petrophysical methods:

Five distinct seismic facies have been distinguished along the seismic dip line PBJ-04. A noticeable shift in facies type, transitioning from Type A (Eocene horizons) to Type B (Miocene horizons), aligns with Shah and Shah (2021) interpretation. This facies transition corresponds to the early phases of salt diapir formation.

The 3D subsurface distribution models unveil a consistent presence of the Lockhart Formation, albeit with faulting in the northwest corner. These models further indicate gradual limbs on the southeast side and steeper limbs on the northwest side of the anticline. Notably, a broad contour enclosure has been identified in the northwest region, hinting at potential areas for hydrocarbon accumulation. High resolution seismic 3D data

Table 6. **Various well logs calculated parameters for different properties estimation**

Depth, ft	Temp	RHOB	ΦD	SP	Φ (N.D)	R_t (LLD)	R_{we}	R_w	*Sw*	SH	Lithology
2624	161	2.64	0.9	–23	0.18	870	0.3	0.6	29%	71%	Limestone
2627	161	2.52	0.8	–21	0.22	1130	0.6	0.7	25%	75%	Limestone
2631	161	2.62	0.9	–26	0.24	1330	0.5	0.6	27%	73%	Limestone
2635	162	2.59	0.9	–32	0.17	1740	0.4	0.6	24%	76%	Limestone
2639	162	2.57	0.7	–39	0.18	1540	0.5	0.7	23%	77%	Limestone
2643	162	2.52	1.1	–33	0.19	931	0.4	0.5	27%	73%	Limestone
2647	163	2.53	1.12	–36	0.17	1080	0.6	0.6	22%	78%	Limestone

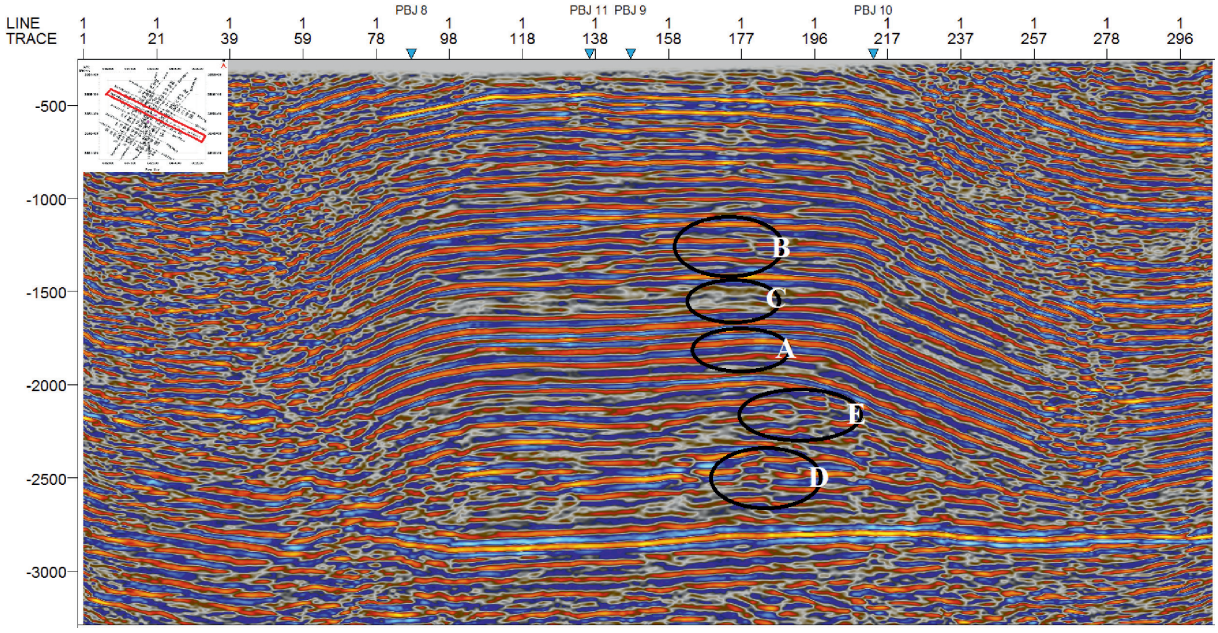

Fig. 13. The identified seismic facies on seismic section PBJ-04.

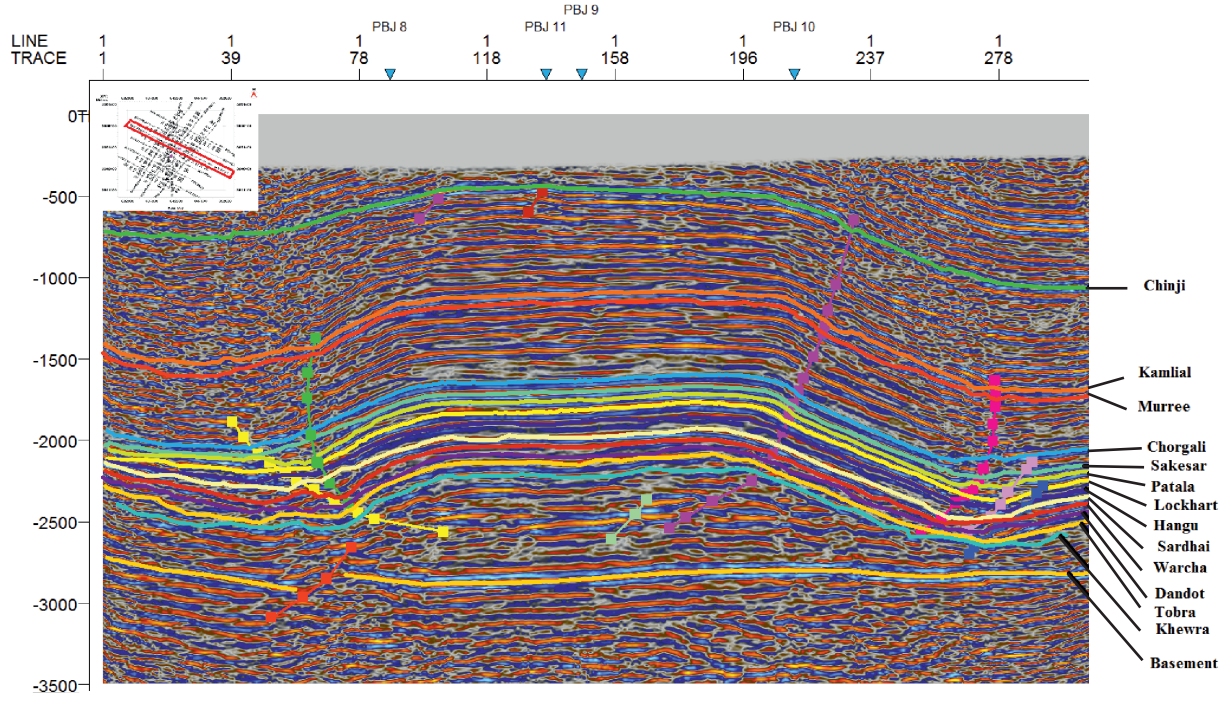

Fig. 14. Interpreted seismic dip line SOX-PBJ-04 by Shah and Shah (2021).

should be acquired for interpretation so that the neglected structure can also be identified. Fault seal analysis should be done for the length of potential prospect. Additionally, Sardhai and Warcha sandstone formations should be evaluated for hydrocarbons.

The examination of Lockhart Formation sediments suggests reasonable hydrocarbon generation potential, as evidenced by S2, HI, and T_{max} values. The sediments display a blend of Type II/III kerogen, inferred from S2 and HI values. Additionally, they fall within the maturity range, signified by both S2 vs TOC and HI vs T_{max} plots. Analysis of Sakesar Formation sediments indicates its aptitude as a reservoir rock rather than a source rock within the Potwar Basin.

In terms of petrophysical analysis, the Lockhart Formation demonstrates average reservoir attributes, while exhibiting favorable potential for hydrocarbon production, highlighted by the percentage of hydrocarbon saturation.

The author is very thankful to University of Malaya, Malaysia for providing lab facilities for this study.

REFERENCES

Aadil, N., Sohail, G.M., 2014. 3D geological modeling of Punjab Platform, Middle Indus Basin Pakistan through integration of Wireline logs and seismic data. J. Geol. Soc. India 83, 211–217, doi: 10.1007/s12594-014-0033-2.

Ahsan, N., Faisal, M. A., Mehmood, T., Ahmed, N., Iqbal, Z., Sameeni, S.J., 2012. 3D modeling of subsurface stratigraphy and structural evolution of Balkassar area, Eastern Potwar, Pakistan. Pakistan J. Hydrocarbon Res. 22 (2), 25–40.

Bordenave, J.E.D., 1999. Alguns fatores pedagógicos. Capacitação em desenvolvimento de recursos humanos. CADRHU, pp. 261–268.

Bordenave, M.L., Espitalié, L., Leplat, P., Oudin, J.L., Vandenbroucke, M., 1993. Screening techniques for source rock evaluation, in: Bordenave, M.L. (Ed.), Applied Petroleum Geochemistry. Editions Technip, Paris, pp. 217–278.

Chen, J., Wen, L., Bi, C., Liu, Z., Liu, X., Yin, L., Zheng, W., 2023. Multifractal analysis of temporal and spatial characteristics of earthquakes in Eurasian seismic belt. Open Geosci. 15, doi: 10.1515/geo-2022-0482.

Cheng, F., Li, J., Zhou, L., Lin, G., 2023. Fragility analysis of nuclear power plant structure under real and spectrum-compatible seismic waves considering soil-structure interaction effect. Eng. Struct. 280, 115684, doi: 10.1016/j.engstruct.2023.115684.

Dang, P., Cui, J., Liu, Q., Li, Y., 2023. Influence of source uncertainty on stochastic ground motion simulation: a case study of the 2022 Mw 6.6 Luding, China, earthquake. Stochastic Environ. Res. Risk Assess. 37, 2943–2960, doi: 10.1007/s00477-023-02427-y.

Fazeelat, T., Jalees, M.I., Bianchi, T.S., 2010. Source rock potential of Eocene, Paleocene and Jurassic deposits in the subsurface of the Potwar Basin, northern Pakistan. J. Petrol. Geol. 33, 87–96. doi: 10.1111/j.1747-5457.2010.00465.x.

Futalan, K., Mitchell, A., Amos, K., Backe, G., 2012. Seismic facies analysis and structural interpretation of the Sandakan sub-basin, Sulu Sea, Philippines, in: Proc. AAPG 2012 Int.Conf. Exhib., 30254.

Hartmann, D.J., Beaumont, E.A., 1999. Predicting reservoir system quality and performance, in: Beaumont, E.A., Foster, N.H. (Eds.), Exploring for Oil and Gas Traps. Treatise of Petroleum Geology. Handbook of Petroleum Geology. AAPG, Tulsa.

He, M., Dong, J., Jin, Z., Liu, C., Xiao, J., Zhang, F., Deng, L., 2021. Pedogenic processes in loess-paleosol sediments: Clues from Li isotopes of leachate in Luochuan loess. Geochim. Cosmochim. Acta 299, 151–162, doi: 10.1016/j.gca.2021.02.021.

Huang, S., Lyu, Y., Sha, H., Xiu, L., 2021. Seismic performance assessment of unsaturated soil slope in different groundwater levels. Landslides 18, 2813–2833, doi: 10.1007/s10346-021-01674-w.

Hunt, J.M., 1996. Petroleum Geochemistry and Geology (2nd ed.). W.H. Freeman and Company, New York.

Ihsan, S., Fazeelat, T., Imtiaz, F., Nazir, A., 2022. Geochemical characteristics and hydrocarbon potential of Cretaceous Upper Shale Unit, Lower Indus Basin, Pakistan. Pet. Sci. Technol. 40, 257–269, doi: 10.1080/10916466.2021.1993913.

Imtiaz, F., Fazeelat, T., Nazir, A., Ihsan, S., 2017. Geochemical characterization of sediments samples of Sembar Formation from three different wells of Southern Indus Basin. Pet. Sci. Technol. 35, 633–640, doi: 10.1080/10916466.2016.1274757.

Iqbal, N., Yaseen, A., Lashari, R., Usmani, P., Ahsan, N., 2015. Some palycepod fossils from Chorgali Formation, Nurpur Area, Central Salt Range, Pakistan. Sindh Univ. Res. J. 43, 181–184.

Kazmi, A.H., Jan, M.Q., 1997. Geology and Tectonics of Pakistan. Graphic Publishers, Karachi, Pakistan.

Kazmi, A.H., Abbasi, I.A., 2008. Stratigraphy and Historical Geology of Pakistan. Department and National Centre of Excellence in Geology, University of Peshawar, Pakistan.

Li, R., Zhang, H., Chen, Z., Yu, N., Kong, W., Li, T., Liu, Y., 2022a. Denoising method of ground-penetrating radar signal based on independent component analysis with multifractal spectrum. Measurement 192, 110886, doi: 10.1016/j.measurement.2022.110886.

Li, R., Wu, X., Tian, H., Yu, N., Wang, C., 2022b. Hybrid memetic pretrained factor analysis-based deep belief networks for transient electromagnetic inversion. IEEE Trans. Geosci. Remote Sens. 60, doi: 10.1109/TGRS.2022.3208465.

Li, Q., Song, D., Yuan, C., Nie, W., 2022c. An image recognition method for the deformation area of open-pit rock slopes under variable rainfall. Measurement 188, 110544, doi: 10.1016/j.measurement.2021.110544.

Li, W., Zhu, J., Fu, L., Zhu, Q., Xie, Y., Hu, Y., 2021. An augmented representation method of debris flow scenes to improve public perception. Int. J. Geogr. Inf. Sci. 35, 1521–1544, doi: 10.1080/13658816.2020.1833016.

Liu, C., Cui, J., Zhang, Z., Liu, H., Huang, X., Zhang, C., 2021. The role of TBM asymmetric tail-grouting on surface settlement in coarse-grained soils of urban area: Field tests and FEA modelling. Tunnelling Underground Space Technol. 111, 103857, doi: 10.1016/j.tust.2021.103857.

Liu, Y., Li, J., Lin, G., 2023a. Seismic performance of advanced three-dimensional base-isolated nuclear structures in complex-layered sites. Eng. Struct. 289, 116247, doi: 10.1016/j.engstruct.2023.116247.

Liu, C., Peng, Z., Cui, J., Huang, X., Li, Y., Chen, W., 2023b. Development of crack and damage in shield tunnel lining under seismic loading: Refined 3D finite element modeling and analyses. Thin-Walled Struct. 185, 110647, doi: 10.1016/j.tws.2023.110647.

Liu, H., Ding, F., Li, J., Meng, X., Liu, C., Fang, H., 2023c. Improved detection of buried elongated targets by dual-polarization GPR. IEEE Geosci. Remote Sens. Lett. 20, doi: 10.1109/LGRS.2023.3243908.

Liu, H., Li, J., Meng, X., Zhou, B., Fang, G., Spencer, B.F., 2022. Discrimination between dry and water ices by full polarimetric radar: Implications for China's first Martian exploration. IEEE Trans. Geosci. Remote Sens. 61, doi: 10.1109/TGRS.2022.3228684.

Liu, Z., Xu, J., Liu, M., Yin, Z., Liu, X., Yin, L., Zheng, W., 2023d. Remote sensing and geostatistics in urban water-resource monitoring: a review. Mar. Freshwater Res., 74, 747–765, doi: 10.1071/MF22167.

Ma, S., Qiu, H., Yang, D., Wang, J., Zhu, Y., Tang, B., Cao, M., 2023. Surface multi-hazard effect of underground coal mining. Landslides 20, 39–52, doi: 10.1007/s10346-022-01961-0.

Masood, F., Ahmad, Z., Khan, M.S., 2017. Moderate interpretation with attribute analysis and 3D visualization for deeper prospects of Balkassar field, Central Potwar, Upper Indus Basin, Pakistan. Int. J. Geosci. 8, 678–692, doi: 10.4236/ijg.2017.85037.

Peng, J., Xu, C., Dai, B., Sun, L., Feng, J., Huang, Q., 2022. Numerical investigation of brittleness effect on strength and microcracking behavior of crystalline rock. Int. J. Geomech. 22, 4022178, doi: 10.1061/(ASCE)GM.1943-5622.0002529.

Peters, K.E., 1986. Guidelines for evaluating petroleum source rock using programmed pyrolysis. AAPG Bull. 70, 318–329, doi: 10.1306/94885688-1704-11D7-8645000102C1865D.

Peters, K.E., Cassa, M.R., 1994. Applied source rock geochemistry, in: Magoon, L.B., Dow, W.G. (Eds.), The Petroleum System – From Source to Trap. AAPG Tulsa, Oklahoma USA, Vol. 60, pp. 93–120).

Ren, C., Yu, J., Liu, S., Yao, W., Zhu, Y., Liu, X., 2022. A plastic strain-induced damage model of porous rock suitable for different stress paths. Rock Mech. Rock Eng. 55, 1887–1906, doi: 10.1007/s00603-022-02775-1.

Ren, C., Yu, J., Zhang, C., Liu, X., Zhu, Y., Yao, W., 2023. Micro–macro approach of anisotropic damage: A semi-analytical constitutive model of porous cracked rock. Eng. Frac. Mech. 290, 109483, doi: 10.1016/j.engfracmech.2023.109483.

Riaz, M., 2022. Subsurface structural interpretation of Missa Keswal, Eastern Potwar, Pakistan. J. Earth Sci. Technol. 3 (Spec. Issue), 17–28.

Rider, M.H., 1986. The Geological Interpretation of Well Logs. John Wiley and Sons, New York, NY.

Schlumberger Log Interpretation Charts, 1977. Schlumberger Limited. New York.

Shah, S.M.I., 2009. Stratigraphy of Pakistan. Government of Pakistan. Ministry of Petroleum and Natural Resources, Geological Survey of Pakistan. Memoirs of the Geological Survey of Pakistan, Vol. 22.

Shah, S.B.A., 2023. Evaluation of organic matter in Sakesar and Patala formations in southern and northern Potwar Basin, Pakistan. Pet. Sci. Technol. 41, 2071–2087, doi: 10.1080/10916466.2022.2105360.

Shah, S.B.A., Abdullah, W.H., 2016. Petrophysical properties and hydrocarbon potentiality of Balkassar well 7 in Balkassar oilfield, Potwar Plateau, Pakistan. Bull. Geol. Soc. Malaysia 62 (1), 73–77.

Shah, S.B.A., Abdullah, W.H., 2017. Structural interpretation and hydrocarbon potential of Balkassar oil field, eastern Potwar, Pakistan, using seismic 2D data and petrophysical analysis. J. Geol. Soc. India 90, 323–328, doi: 10.1007/s12594-017-0720-x.

Shah, S.B.A., Shah, S.H.A., 2021. Hydrocarbon generative potential of Cretaceous and Jurassic deposits in the Ahmedpur East Oilfield Subsurface, Punjab Platform, Pakistan. J. Geol. Soc. India 97, 923–926, doi: 10.1007/s12594-021-1792-1.

Sun, X., Chen, Z., Sun, Z., Wu, S., Guo, K., Dong, Z., Peng, Y., 2023a. High-efficiency utilization of waste shield slurry: A geopolymeric flocculation–filtration–solidification method. Constr. Build. Mater. 387, 131569, doi: 10.1016/j.conbuildmat.2023.131569.

Sun, X., Chen, Z., Guo, K., Fei, J., Dong, Z., Xiong, H., 2023b. Geopolymeric flocculation-solidification of tail slurry of shield tunnelling spoil after sand separation. Constr. Build. Mater. 374, 130954. doi: 10.1016/j.conbuildmat.2023.130954.

Wang, W., Li, D., Tang, X., Du, W., 2023. Seismic fragility and demand hazard analyses for earth slopes incorporating soil property variability. Soil Dyn. Earthquake Eng. 173, 108088, doi: 10.1016/j.soildyn.2023.108088.

Wu, M., Ba, Z., Liang, J., 2022a. A procedure for 3D simulation of seismic wave propagation considering source-path-site effects: Theory, verification and application. Earthquake Eng. Struct. Dyn. 51, 2925–2955, doi: 10.1002/eqe.3708.

Wu, Z., Xu, J., Li, Y., Wang, S., 2022b. Disturbed state concept–based model for the uniaxial strain-softening behavior of fiber-reinforced soil. Int. J. Geomech. 22, 4022092, doi: 10.1061/(ASCE)GM.1943-5622.0002415.

Xiao, D., Liu, M., Li, L., Cai, X., Qin, S., Gao, R., Li, G., 2023. Model for economic evaluation of closed-loop geothermal systems based on net present value. Appl. Therm. Eng. 231, 121008, doi: 10.1016/j.applthermaleng.2023.121008.

Xu, J., Lan, W., Ren, C., Zhou, X., Wang, S., Yuan, J., 2021. Modeling of coupled transfer of water, heat and solute in saline loess considering sodium sulfate crystallization. Cold Reg. Sci. Technol. 189, 103335, doi: 10.1016/j.coldregions.2021.103335.

Xu, Z., Wang, Y., Jiang, S., Fang, C., Liu, L., Wu, K., Chen, Y., 2022a. Impact of input, preservation and dilution on organic matter enrichment in lacustrine rift basin: A case study of lacustrine shale in Dehui Depression of Songliao Basin, NE China. Mar. Petrol. Geol. 135, 105386, doi: 10.1016/j.marpetgeo.2021.105386.

Xu, Z., Li, X., Li, J., Xue, Y., Jiang, S., Liu, L., Sun, Q., 2022b. Characteristics of source rocks and genetic origins of natural gas in deep formations, Gudian depression, Songliao Basin, NE China. ACS Earth Space Chem. 6, 1750–1771, doi: 10.1021/acsearthspacechem.2c00065.

Yang, D., Qiu, H., Ye, B., Liu, Y., Zhang, J., Zhu, Y., 2023. Distribution and recurrence of warming-induced retrogressive thaw slumps on the Central Qinghai-Tibet Plateau. J. Geophys. Res.: Earth Surf. 128, e2022JF007047, doi: 10.1029/2022JF007047.

Yang, J., Fu, L., Fu, B., Deng, W., Han, T., 2022. Third-order Padé thermoelastic constants of solid rocks. J. Geophys. Res.: Solid Earth 127, e2022JB024517, doi: 10.1029/2022JB024517.

Yao, W., Yu, J., Liu, X., Zhang, Z., Feng, X., Cai, Y., 2023. Experimental and theoretical investigation of coupled damage of rock under combined disturbance. Int. J. Rock Mech. Min. Sci. 164, 105355, doi: 10.1016/j.ijrmms.2023.105355.

Yasin, Q., Baklouti, S., Khalid, P., Ali, S.H., Boateng, C.D., Du, Q., 2021. Evaluation of shale gas reservoirs in complex structural enclosures: A case study from Patala Formation in the Kohat-Potwar Plateau, Pakistan. J. Pet. Sci. Eng. 198, 108225, doi: 10.1016/j.petrol.2020.108225.

Yin, L., Wang, L., Ge, L., Tian, J., Yin, Z., Liu, M., Zheng, W., 2023a. Study on the thermospheric density distribution pattern during geomagnetic activity. Appl. Sci. 13, 5564, doi: 10.3390/app13095564.

Yin, H., Wu, Q., Yin, S., Dong, S., Dai, Z., Soltanian, M.R., 2023b. Predicting mine water inrush accidents based on water level anomalies of borehole groups using long short-term memory and isolation forest. J. Hydrol. 616, 128813, doi: 10.1016/j.jhydrol.2022.128813.

Yin, H., Zhang, G., Wu, Q., Yin, S., Soltanian, M.R., Thanh, H.V., Dai, Z., 2023. A deep learning-based data-driven approach for predicting mining water inrush from coal seam floor using microseismic monitoring data. IEEE Trans. Geosci. Remote Sens. 61, doi: 10.1109/TGRS.2023.3300012.

Yu, J., Zhu, Y., Yao, W., Liu, X., Ren, C., Cai, Y., Tang, X., 2021. Stress relaxation behaviour of marble under cyclic weak disturbance and confining pressures. Measurement 182, 109777, doi: 10.1016/j.measurement.2021.109777.

Yuan, C., Li, Q., Nie, W., Ye, C., 2023. A depth information-based method to enhance rainfall-induced landslide deformation area identification. Measurement 219, 113288, doi: 10.1016/j.measurement.2023.113288.

Zahid, M., Khan, A., ur Rashid, M., Saboor, A., Ahmad, S., 2014. Structural interpretation of Joya Mair oil field, south Potwar, Upper Indus Basin, Pakistan, using 2D seismic data and petrophysical analysis. J. Himalayan Earth Sci. 47 (1), 73–86.

Zhan, C., Dai, Z., Soltanian, M.R., de Barros, F.P.J., 2022. Data-worth analysis for heterogeneous subsurface structure identification with a stochastic deep learning framework. Water Resour. Res. 58, e2022WR033241, doi: 10.1029/2022WR033241.

Zhang, K., Wang, Z., Chen, G., Zhang, L., Yang, Y., Yao, C., Yao, J., 2022a. Training effective deep reinforcement learning agents for real-time life-cycle production optimization. J. Pet. Sci. Eng. 208, 109766, doi: 10.1016/j.petrol.2021.109766.

Zhang, Y., Luo, J., Zhang, Y., Huang, Y., Cai, X., Yang, J., Zhang, Y., 2022b. Resolution enhancement for large-scale real beam mapping based on adaptive low-rank approximation. IEEE Trans. Geosci. Remote Sens. 60, 1–21, doi: 10.1109/TGRS.2022.3202073.

Zhao, Z., Xu, G., Zhang, N., Zhang, Q., 2022. Performance analysis of the hybrid satellite-terrestrial relay network with opportunistic scheduling over generalized fading channels. IEEE Trans. Veh. Technol. 71, 2914–2924, doi: 10.1109/TVT.2021.3139885.

Zhao, M., Zhou, Y., Li, X., Cheng, W., Zhou, C., Ma, T., Huang, K., 2020. Mapping urban dynamics (1992–2018) in Southeast Asia using consistent nighttime light data from DMSP and VIIRS. Rem. Sens. Environ. 248, 111980, doi: 10.1016/j.rse.2020.111980.

Zheng, Z., Zuo, Y., Wen, H., Li, D., Luo, Y., Zhang, J., Zeng, J., 2023. Natural gas characteristics and gas-source comparisons of the lower Triassic Feixianguan formation, Eastern Sichuan basin. Pet. Sci. 20, 1458–1470, doi: 10.1016/j.petsci.2023.02.005.

Zhou, L., Ye, Y., Tang, T., Nan, K., Qin, Y., 2022a. Robust matching for SAR and optical images using multiscale convolutional gradient features. IEEE Geosci. Remote Sens. Lett. 19, 1–5. doi: 10.1109/LGRS.2021.3105567.

Zhou, G., Zhou, X., Song, Y., Xie, D., Wang, L., Yan, G., Wang, H., 2021a. Design of supercontinuum laser hyperspectral light detection and ranging (LiDAR) (SCLaHS LiDAR). Int. J. Remote Sens. 42, 3731–3755, doi: 10.1080/01431161.2021.1880662.

Zhou, G., Deng, R., Zhou, X., Long, S., Li, W., Lin, G., Li, X., 2021b. Gaussian inflection point selection for LiDAR hidden echo signal decomposition. IEEE Geosci. Remote Sens. Lett. 19, doi: 10.1109/LGRS.2021.3107438.

Zhou, G., Zhang, R., Huang, S., 2021c. Generalized buffering algorithm. IEEE Access 9, 27140–27157, doi: 10.1109/ACCESS.2021.3057719.

Zhou, S., Lu, C., Zhu, X., Li, F., 2021d. Preparation and characterization of high-strength geopolymer based on BH-1 lunar soil simulant with low alkali content. Engineering 7, 1631–1645, doi: 10.1016/j.eng.2020.10.016.

Zhuo, Z., Du, L., Lu, X., Chen, J., Cao, Z., 2022. Smoothed Lv distribution based three-dimensional imaging for spinning space debris. IEEE Trans. Geosci. Remote Sens. 60, 1–13, doi: 10.1109/TGRS.2022.3174677.